

GT2011-45) \$\$

IMPROVING THE APPLICATION OF TURBINE MAPS IN 1D ENGINE PROCESS MODELLING

Mathias Vogt

Voith Turbo Aufladungssysteme GmbH & Co KG
 Gommern, Germany

Holger Mai

Technische Universität Berlin
 Berlin, Germany

Florian Frese

Voith Turbo Aufladungssysteme GmbH & Co KG
 Gommern, Germany

Roland Baar

Voith Turbo Aufladungssysteme GmbH & Co KG
 Gommern, Germany

ABSTRACT

The new Euro 6 emission limits represent a major challenge to the development of internal combustion engines. One way to achieve this goal is to enhance the 1D engine process simulation of supercharged engines. In contrast to the widely-used 1D-modelling of pipe flow, turbochargers are generally modelled using maps of mass flow and efficiency. The turbines of turbochargers are usually mapped with constant back pressure and constant inlet temperature on special test beds. Standard non-dimensional values for flow and impeller speed should allow the turbine operating point to be recalculated depending on its boundary conditions. This procedure does not work sufficiently for operating conditions that, e.g. occur in two stage turbocharging or at high temperature offsets to the mapping conditions. This especially concerns the turbine efficiency. Methods like varying the turbine inlet temperature and the turbine back pressure expand the information of the turbine characteristic map. Both methods, used as additional boundary conditions, improve the precision of 1D simulation. The effects of the adjustments will be demonstrated using the example of a 1D engine process simulation of a turbocharged engine.

NOMENCLATURE

A	Area
BC	Boundary condition
BSR	Blade speed ratio
C	Compressor
c	Fluid velocity
c_0	Isentropic velocity
cm	Meridional velocity

cu	Circumferential fluid velocity
CFD	Computational fluid dynamics
d	Diameter
EGR	Exhaust gas recirculation
K	Loss coefficient
Ma	Mach number
n	Speed
N	Nodes
OP	Operating points
p	Pressure
s	Entropy
SST	Shear-stress-transport
T	Temperature
u	Circumferential velocity
r	Radius of centre of area
r	Residual of variable
w	Relative velocity
wu	Circumferential relative velocity
Z	Efficiency correlation factor

Greek Letters

α	Absolute flow angle
β	Relative flow angle
Δ	Delta
η	Efficiency
Θ	Angle
v	Variable
Π	Pressure ratio
ρ	Density
ϕ	Reduced mass flow
ω_x	Streamwise vorticity

Subscripts

1	Compressor inlet (measuring point)
2	Compressor outlet (measuring point)
3	Turbine inlet (measuring point)
3.1	Passage Area
3.3	Rotor inlet
4	Turbine outlet (measuring point)
abs	Absolute
is	Isentropic
red	Reduced
RMS	Root mean square
m	Mechanical
m	Measured
max	Maximum
R	Rotor
s	Simulated
s	Static
T	Turbine
TC	Turbocharger
t	Total
t-s	Total to static
τ	Temperature
V	Volute

Operator

∇	Nabla operator
----------	----------------

INTRODUCTION

In light of shorter development cycles and tighter emission regulations, the importance of engine process simulation increases in the development process of internal combustion engines. The accuracy of the engine process simulation of turbocharged engines is highly dependent on the quality of the modelling of the charging units.

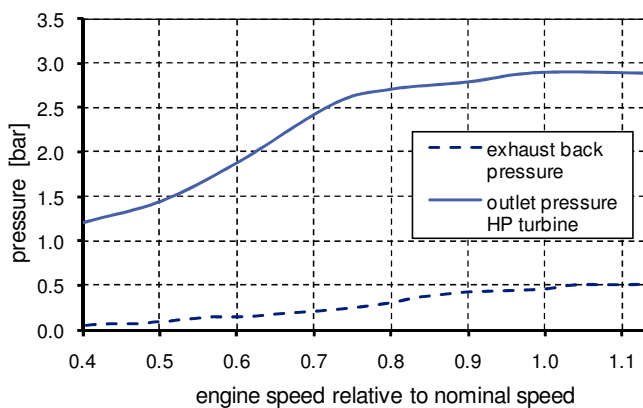


Figure 1: Back pressure of exhaust system and 2-stage HP turbine outlet pressure

The challenges in description of turbocharger turbine behavior arise from pulsating exhaust mass flow of reciprocating engines, imprecise determination of mechanical losses and the variation of turbine inlet temperature and turbine back pressure. The paper concentrates on the effects of the latter two components.

Turbocharger turbine characteristics are usually mapped with constant absolute back pressure ($p_{4abs} = 1\text{bar}$) close to ambient pressure on special steady flow hot gas test beds. In contrast, modern turbochargers running on Diesel engines encounter higher values of back pressure not only through exhaust gas after-treatment systems, like Diesel particulate filters or catalysts, but also through turbines running downstream the considered aggregate.

Figure 1 shows an example of full load pressure profiles of actual Diesel engines. The exhaust back pressure reaches a maximum of approximate 500 mbar due to flow-related losses in the catalyst, the Diesel particulate filter and in the following exhaust pipes. The high pressure (HP) turbine outlet pressure of the 2-stage turbocharger system rises to 2.9 bar. This engine is highly supercharged to realise exhaust gas recirculation (EGR) rates of up to 45 %. The procedure of inducing cooled exhaust gas into the compressed fresh air leads to reduced maximum cylinder temperatures because of the capacitive effect of the inert gas. This lowers the nitrogen oxide emissions of the engine.

These two examples show that turbocharger turbines can operate far beyond usual test conditions with regard to their outlet pressure. This paper examines how this modified boundary condition affects the efficiency of the turbo-machine.

The turbine inlet temperature of steady flow hot gas test beds is commonly set to 873 K for turbochargers of Diesel engines and often even for turbochargers of SI engines. Sometimes, the turbine inlet temperature is alternatively set to 1223 K for turbochargers of SI engines.

Figure 2 shows the real turbine inlet temperatures of Diesel and SI engines. The spread from lower part load operating conditions to full load operating conditions ranges up to 570 K, which is quite large in view of the impact on the amount of heat flux [1], [2].

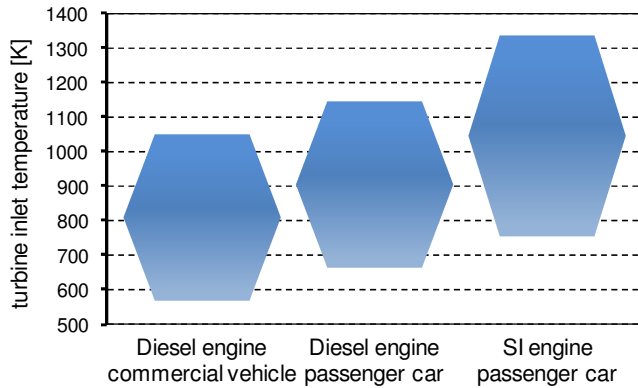


Figure 2: Turbine inlet temperatures of Diesel and SI engines

INFLUENCE OF BACK PRESSURE

Experimental Investigation

Several turbines with different sizes of turbine wheel were analysed on a hot gas test bed under steady state conditions to investigate the turbine back pressure. To realise different back pressures, a valve is used that is located behind the turbine outlet and outside of the system boundary. A schematic overview of the measurement setup can be seen in Figure 3. The temperature and pressure values and so the depending caloric values for the turbine and compressor inlet and outlet are measured on the system boundary.

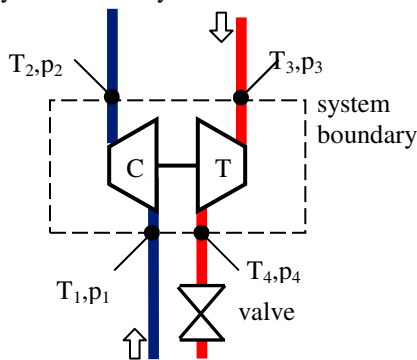
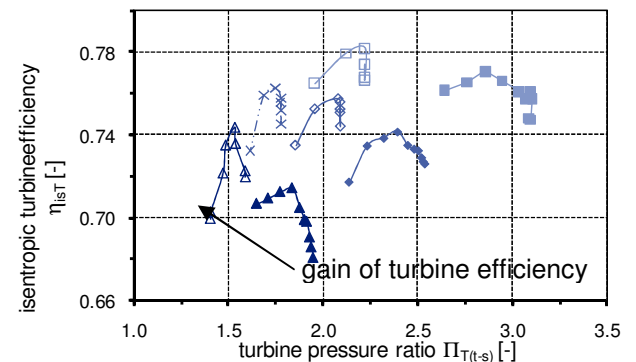
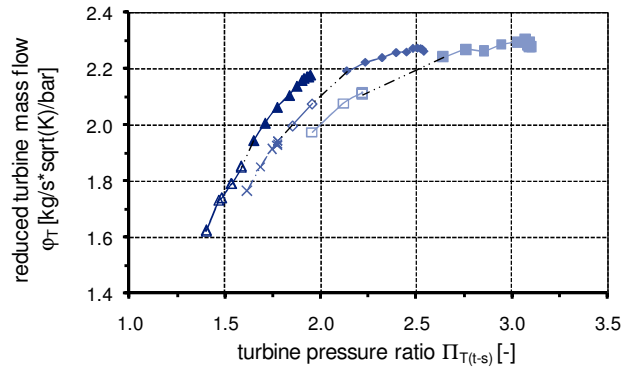


Figure 3: Schematic view of a turbocharger at hot gas test bed

Figure 4 shows a turbine performance map of a twin scroll turbine that has a turbine wheel diameter of $d_T = 70$ mm. This turbine is designed for heavy duty Diesel engines. The turbine was investigated under equal admission. During the test programme the back pressure is constant at each speed line and varies from $p_{4abs} = 1$ bar to $p_4 = 2.5$ bar.



- ▲— $n_{Tred}=2708 \text{min}^{-1} \text{K}^{-0.5}; p_{4abs}=1 \text{bar}$
- △— $n_{Tred}=2708 \text{min}^{-1} \text{K}^{-0.5}; p_{4abs}=2 \text{bar}$
- ◆— $n_{Tred}=3384 \text{min}^{-1} \text{K}^{-0.5}; p_{4abs}=1 \text{bar}$
- ◇— $n_{Tred}=3384 \text{min}^{-1} \text{K}^{-0.5}; p_{4abs}=1.5 \text{bar}$
- ×— $n_{Tred}=3384 \text{min}^{-1} \text{K}^{-0.5}; p_{4abs}=2.5 \text{bar}$
- $n_{Tred}=3891 \text{min}^{-1} \text{K}^{-0.5}; p_{4abs}=1 \text{bar}$
- $n_{Tred}=3891 \text{min}^{-1} \text{K}^{-0.5}; p_{4abs}=2 \text{bar}$

Figure 4: Turbine performance map for a heavy duty Diesel engine with increased back pressure at turbine outlet and constant inlet temperature ($T_3=873\text{K}$)

By increasing the turbine back pressure the speed lines are shifted to a lower turbine pressure ratio and to a lower reduced mass flow (Figure 4 a). Currently, the isentropic turbine efficiency rises (Figure 4 b). With this technique the turbine map can be expanded and the turbine efficiency can be improved.

The isentropic turbine efficiency is calculated by the following equation (1)

$$\eta_{isT} = \frac{\eta_{TC}}{\eta_m \cdot \eta_{isC}} \quad (1)$$

Normally the turbine efficiency is a product of the isentropic turbine efficiency and the mechanical efficiency. To separate the mechanical loss a “cold” turbine map was investigated in which

the turbine inlet temperature is equal to the compressor outlet temperature and the oil temperature is constant to minimize the heat transfer in the turbocharger. By measuring the oil inlet and outlet temperature and the oil mass flow the mechanical power can be calculated, in which the rise of the oil outlet temperature is caused only by the friction of the turbocharger shaft and not from the heat transfer [3].

CFD-Analysis

Numerical Setup and Grid Analysis

The numerical investigation for the influence of the turbine back pressure was carried out with the CFD programme ANSYS CFX 11.0. The investigation should show how the increased back pressure influence the aerodynamic loss and the general turbine behaviour. The CFD model was divided into four domains, whereas the inlet and the outlet paths were modelled to take into account the flow loss from the measuring point to the inlet of the turbine housing and from the outlet of the turbine to the measuring point. The four domains were:

- Inlet
- Volute
- Rotor
- Outlet

For the rotor, the inlet and the outlet a hexahedral mesh was used. Because of the geometric complexity, the volute was meshed with an unstructured tetrahedral and prism mesh to resolve the boundary layer. A dimensionless wall distance of one was reached to solve the boundary layer.

Before the CFD analysis, a grid study was done to check the grid sensitivity with regard to the results. Therefore, three grids were created with a different number of cells (Table 1) that have a minimum orthogonal angle of 21 degrees and a maximum mesh expansion factor of 19 to ensure adequate grid quality.

Table 1: Overview of grid study and final grid

	grid 1	grid 2	grid 3	final grid
	Elements	Elements	Elements	Elements
Inlet	2142084	1560024	1009080	1560024
Volute	10387932	6174541	4927371	6174541
Rotor	10306510	7446550	5476240	7446550
Outlet	3822006	2865644	1955940	2865644
Σ Elements	26658532	18046759	13368631	18046759

In addition to the grid analysis, the influence of the numerical discretisation schemes was investigated. Therefore, an upwind and a high resolution advection scheme were used to evaluate the results compared to a first order and an automatic differencing scheme. The high resolution scheme uses a blend factor between 0.0 and 1.0. When this blend factor is 0.0, the advection scheme becomes 1st order, and 2nd order when its

value is 1.0. The selection of the blend factor depends on the variable gradients. When the gradients are low a factor close to 1.0 is chosen; when the gradients are high a blend factor close to 0.0 is chosen to prevent overshoots and undershoots and to produce robustness [4]. Convergence is reached when the target values, e.g. mass flow rate, are in a steady state, which means no change over iteration and the imbalances are zero and the normalised maximum residuals (MAX residual) below $1.0 \cdot 10^{-2}$. The normalised residual for each solution variable v is calculated as follows:

$$[\tilde{r}_v] = [r_v] / a_p \Delta v \quad (2)$$

Thereby, r_v is the raw residual control volume imbalance, a_p is representative of the control volume coefficient and Δv is a representative range of the variable in the domain [4]. The variable v could be a maximum absolute value (MAX residual) for all grid points or a root mean value (RMS residual). The MAX and RMS residuals are calculated by equation (3) and (4) where N stands for grid points.

$$[\tilde{r}_{vmax}] = \max(|\tilde{r}_v|) \quad (3)$$

$$[\tilde{r}_{vrms}] = \sqrt{\frac{1}{N} \sum \tilde{r}_v^2} \quad (4)$$

The MAX residual is a stronger convergence criterion. The steady state CFD results presume that the flow field is unsteady and this could be the reason why the residuals are only at $1.0 \cdot 10^{-2}$. A transient CFD analysis was thus performed. This analysis has shown that the residuals could be reduced further to $1.0 \cdot 10^{-4}$ but the integral values like mass flow or temperature drop have nearly the same value as the steady state simulation.

After the preliminary study, a final grid (Table 1) was chosen that represented a good compromise between computational time and flow field resolution.

All CFD simulations used the same type of boundary conditions. For the steady state analysis, a frozen rotor interface was used to connect the rotor with the volute. The walls were modelled as adiabatic and frictionless and the measured data from the test rig for total pressure and total temperature at the inlet, the static pressure at the outlet, and the turbocharger revolution for the turbine wheel, were used as boundary conditions. For the investigations, the high resolution advection scheme and the two equation Shear-Stress-Transport (SST) turbulence model were used, which shows a good compromise between numerical effort and computational accuracy [4].

By using the pressure boundary condition, the mass flow or reduced turbine mass flow (ϕ_T) and the turbine outlet

temperature (T_{4s}) were a numerical result of the CFD simulation. The maximum mass flow deviation is 4 % and the maximum turbine outlet temperature deviation is 3 %, which are acceptable values regarding measurement, numerical and modelling errors. Table 2 gives an overview of the numerical accuracy at two selected turbine operating points (OP).

Table 2: Overview of CFD accuracy compared to test bed

		operating point 1		operating point 2	
		BC	$\frac{(v_m - v_s)}{v_m}$	BC	$\frac{(v_m - v_s)}{v_m}$
n_{TC}	[min^{-1}]*1000	100.0		115.0	
p_{3t}	[bar]	2.11		2.83	
T_{3t}	[K]	873.31		872.41	
p_{4s}	[bar]	0.99		1.02	
$\Pi_{T(t-s)}$	[-]	2.14		2.76	
T_{4s}	[K]	736.6	-2.2%	705.5	-0.7%
Φ_T	[$\text{kg/s} \cdot \text{K}^{0.5}/\text{bar}$]	2.19	-2.5%	2.27	-2.2%
η_{isT}	[-]	0.86	4.6%	0.80	-4.4%

CFD Results

The experimental investigation shows that the operating range of the turbine is shifted by increasing the back pressure. In this case the increased p_4 produces a higher u/c_0 ratio (blade speed ratio BSR) compared to a turbine that expands to an ambient pressure boundary condition at the turbine outlet. With a BC of $p_{4abs} = 1\text{bar}$ the investigated turbine has a u/c_0 ratio from 0.45 to 0.60. Under the influence of a higher back pressure the u/c_0 ratio reaches values up to 0.70.

A numerical study by CFD was done to investigate a turbine under the influence of variable back pressure with a constant turbine total to static pressure ratio and constant turbocharger speed. This case could occur, for example, for a high pressure turbine for a two stage turbocharger system. Therefore, the absolute pressure at the turbine outlet (p_{4abs}) varies from 1 bar (ambient conditions) to 3 bar. The turbine inlet pressure is adjusted to realise a constant turbine pressure ratio. The investigated points for the study are shown in Table 3.

Table 3: Selected operating points at turbine inlet temperature of 873 K

	p_{3t}	p_{4abs}	$n_{T\text{red}}$	Φ_T	$\Pi_{T(t-s)}$
	[bar]	[bar]	[$\text{min}^{-1}\text{K}^{-0.5}$]	[$\text{kg/s} \cdot \text{K}^{0.5}/\text{bar}$]	[-]
1	1.71	1.00	3384	1.98	1.71
2	3.42	2.00	3384	1.99	1.71
3	5.13	3.00	3384	2.00	1.71
4	2.49	1.00	3891	2.32	2.49
5	4.98	2.00	3891	2.32	2.49
6	7.47	3.00	3891	2.32	2.49

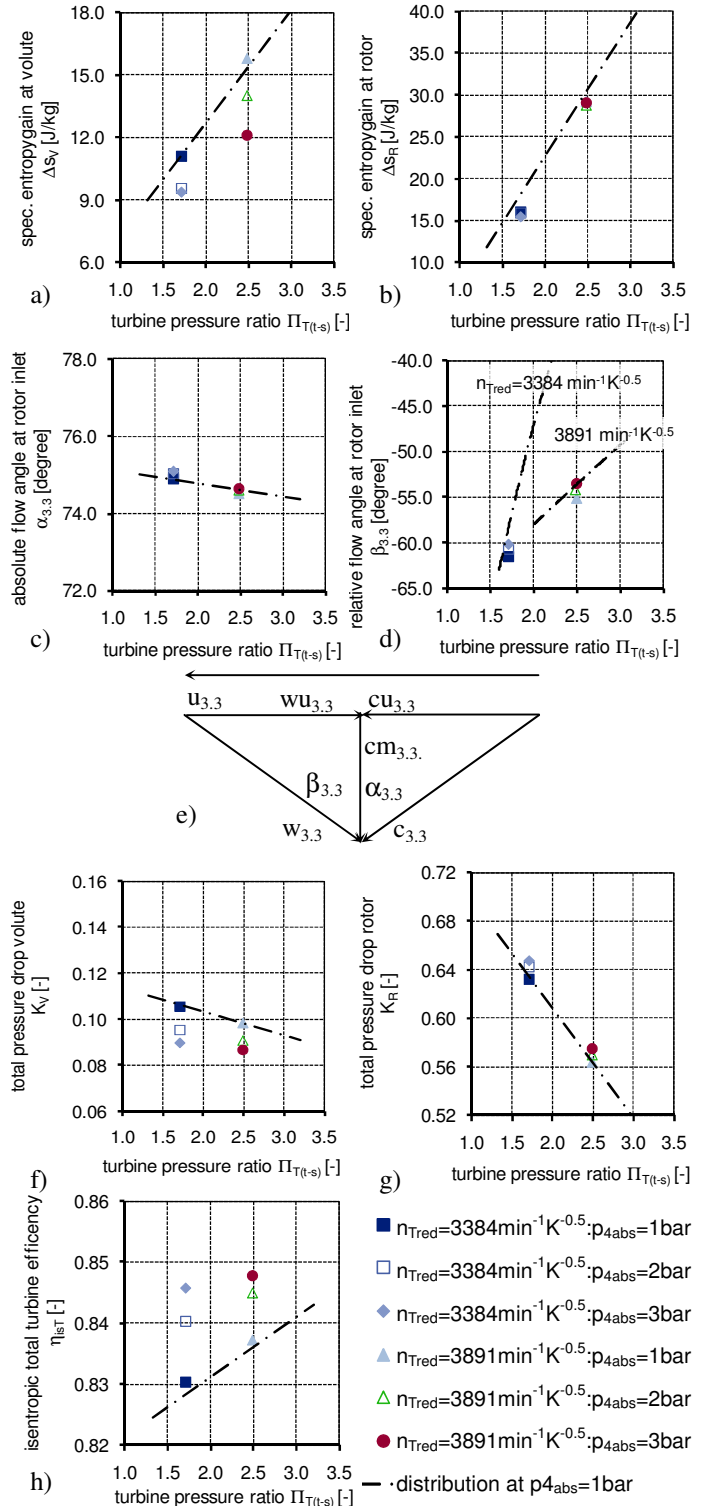


Figure 5: a) Specific entropy gain at turbine volute; b) Specific entropy gain at turbine rotor; c) Absolute flow angle distribution; d) Relative flow angle distribution; e) Velocity triangle; f) Total pressure drop at turbine volute; g) Total pressure drop at turbine rotor; h) Isentropic total turbine efficiency

The numerical study shows such as the measurements that a higher back pressure causes higher isentropic turbine efficiency (Figure 5 h). In both cases the loss distribution is nearly the same and will be characterised by the entropy gain at the turbine volute and at the turbine wheel. Figure 5 a shows the entropy gain at the volute versus the turbine total to static pressure ratio. The dashed dotted line shows the entropy distribution for the turbine outlet condition $p_{4abs} = 1$ bar.

It could be noted that with an increasing p_4 from 1 to 3 bar the production of entropy could be reduced. A reduction in the entropy of 15 % has been reached at $\Pi_{T(t-s)} = 1.71$ and 23 % of the entropy could be reduced at $\Pi_{T(t-s)} = 2.49$. In contrast, the flow loss at the turbine wheel is almost constant and will not be influenced by increased back pressure (Figure 5 b).

The flow angle of incoming flow on the turbine wheel has a significant influence on the energy transformation of the turbine. [4] showed in his work that the relative flow angle has a significant influence on the turbine efficiency. Figure 5 c and d show the distribution of the mass and circumferential averaged absolute flow angle ($\alpha_{3,3}$) and the mass and circumferential averaged relative flow angle ($\beta_{3,3}$) in front of the wheel. The diagrams illustrate that only the absolute flow angle is not influenced by the back pressure. The absolute flow angle is generally influenced by the geometric behavior of the turbine volute, especially by the volute passage area and the rotor inlet area. Based on the volute flow changes in static pressure lead to changes in density which caused marginal changes in the absolute flow angle (5).

$$\tan \alpha_{3,3} = \frac{cm_{3,3}}{cu_{3,3}} = \frac{r_{3,3}}{r_{3,1}} \cdot \frac{\varphi_{3,1}}{\varphi_{3,3}} \cdot \frac{A_{3,1}}{A_{3,3}} \quad (5)$$

In contrast to the absolute flow angle, the relative flow angle is influenced by the operating conditions especially by the mass flow. By a higher back pressure at constant rotor speed, the absolute mass flow rises in which the velocity triangle is shifted proportional, whereby the relative flow angle is shifted marginally to higher values so that the approaching flow in the rotor is almost constant by the investigated operating points. With the help of the schematic velocity triangle in Figure 5 e the definition of the flow angle could be seen.

The total pressure drop coefficient provides information about the amount of pressure drop in the volute (K_v) and the rotor (K_R).

$$K_v = \frac{\Delta p_{vt}}{0.5 \cdot \rho_{3,1} \cdot c_0^2} \quad (6)$$

$$K_R = \frac{\Delta p_{Rt}}{0.5 \cdot \rho_{3,1} \cdot c_0^2} \quad (7)$$

The loss coefficients are given by the equations (6) and (7) in which the total pressure difference in the volute (Δp_{vt}) and in

the rotor (Δp_{Rt}) is divided by the kinetic energy which occurs due to an isentropic expansion with the velocity c_0 . The total pressure drop for the volute and rotor can be seen in Figure 5 f and g. Similar to the entropy gain, the results show that the flow loss can be more reduced in the volute than the rotor.

A reduced flow loss in the volute domain is caused by a lower vorticity production, which is evoked by an increase in p_4 . The streamwise vorticity (ω_x)

$$\omega_x = (\nabla \times \vec{c}) \cdot \vec{c} \quad (8)$$

will be calculated by the scalar product of the vorticity ($\nabla \times \vec{c}$) and fluid velocity (\vec{c}). The streamwise vorticity provides a statement about the vorticity transport, which occurs normally with flow direction.

Figure 6 a and b show the streamwise vorticity distribution in the two scrolls of the turbine volute versus the volute angle Θ_v for the OP by $\Pi_{T(t-s)} = 1.71$ and $\Pi_{T(t-s)} = 2.49$. Each diagram shows the streamwise vorticity distribution for the scroll a and b for $p_4 = 1$ bar (blue line) and for $p_4 = 3$ bar. The positive and negative signs stand for different rotational directions that occur at the different pressure gradients at each scroll. The angle $\Theta_v = 0$ degree represents the position of the volute passage area. The results show that the production of vortices can be reduced by a higher back pressure at the end of the volute.

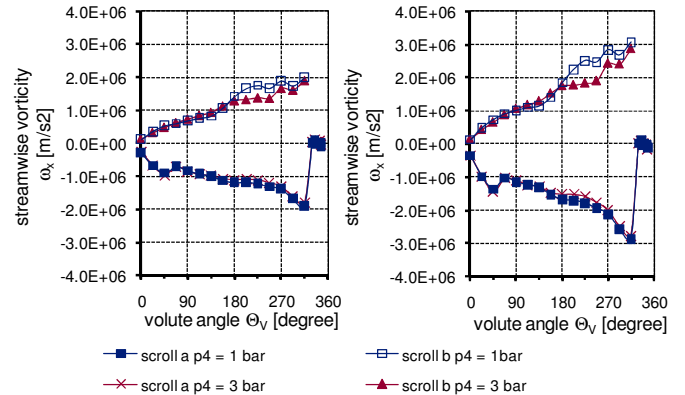


Figure 6: Streamwise vorticity distribution at volute:

a) $\Pi_{T(t-s)} = 1.71$

b) $\Pi_{T(t-s)} = 2.49$

In essence, it can be deduced from Figure 5 h that a growing turbine back pressure has less impact on the isentropic turbine efficiency, with increasing turbine pressure ratio. According to the shown CFD-Results a turbine efficiency correlation factor Z_p for turbine back pressure can be implemented:

Table 4: Turbine efficiency correlation factor Z_p depending on absolute turbine back pressure and turbine pressure ratio

Z_p	$p_{4s} = 1 \text{ bar}$	$p_{4s} = 2 \text{ bar}$	$p_{4s} = 3 \text{ bar}$
$\Pi_{T(t-s)}=1.71$	1	1.0119	1.0185
$\Pi_{T(t-s)}=2.49$	1	1.0093	1.0125

INFLUENCE OF TURBINE INLET TEMPERATURE

Due to different turbine design and size, the performance characteristics of a turbine will be expressed in terms of dimensionless numbers, e.g. turbine pressure ratio, blade speed ratio and turbine efficiency. All the independent measurement variables of the turbine can be transferred into these characteristic parameters.

To represent the exhaust gas flow capacity of the turbine, a flow parameter is usually defined that describes the characteristics of the turbine in the turbine map. This turbine mass flow parameter corresponds to the equivalent of a throttle cross-section. In this way, it is possible to simplify the comparison of different flow rates in turbine maps that were measured at different conditions of pressure and temperature. The turbine mass flow is primarily a function of fluid velocity and density and has a relation to the speed of sound as shown in equation (9).

$$Ma = \frac{c_3}{a} = \frac{\dot{m}_T}{\rho_3 \cdot A} \quad \text{and} \quad \rho_3 = \frac{p_3}{R \cdot T_3} \quad (9)$$

Assuming the use of ideal gas, the isentropic exponent, the gas constant R and the cross section area are constant and can be omitted. Thus, the equation becomes

$$Ma \sim \frac{\dot{m}_T \cdot T_3}{\sqrt{p_3}} = \frac{\dot{m}_T \cdot \sqrt{T_3} \cdot \sqrt{T_3}}{\sqrt{p_3}} = \frac{\dot{m}_T \cdot \sqrt{T_3}}{\sqrt{p_3}} = \varphi_T \quad (10)$$

As a consequence of equation (8) at constant pressure p_3 at turbine inlet, the turbine mass flow changes with $T^{0.5}$, while at constant turbine inlet temperature T_3 the turbine mass flow is directly proportional to the pressure p_3 . This is confirmed by experimental data shown in Figure 7.

The variation of turbine inlet temperature represents (in addition to a variation of turbine back pressure) another way to extend the turbine map. The range of turbine inlet temperature is between 673 K (diamond), 873 K (circle) and 1073 K (triangle). It can be seen that a temperature variation at turbine inlet has no influence on the turbine flow characteristics expressed in the reduced turbine mass flow. Characteristics with the same reduced turbine speed cause an extrapolation to higher turbine pressure ratios at higher turbine inlet temperatures (1073 K). Lower turbine inlet temperatures (673 K) extend the curve of constant reduced turbine speed down to lower turbine pressure ratios.

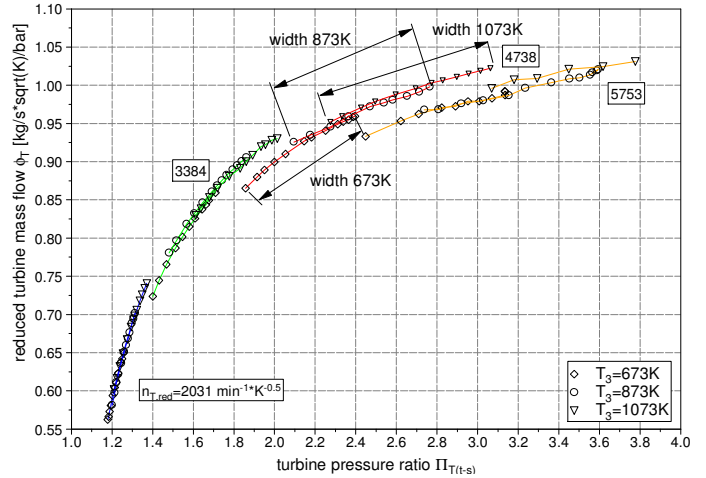


Figure 7: Turbine map – mass flow vs. pressure ratio

The turbine flow characteristic is shown in the turbine map - BSR vs. pressure ratio (Figure 8). Due to lower turbine inlet temperature the blade speed ratio increases at constant reduced turbine speed. In the range of BSR=0.707 is the isentropic turbine efficiency [10] and thus the turbine efficiency maximum.

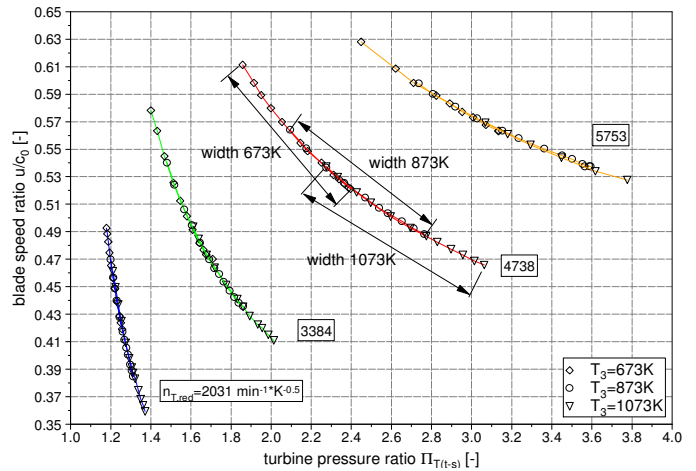


Figure 8: Turbine map – BSR vs. pressure ratio

Figure 9 shows the influence of turbine inlet temperature variation on turbine efficiency at four constant reduced turbine speeds ($n_{T,red} = 3384, 4738, 5753 \text{ min}^{-1}\text{K}^{-0.5}$). There is a significant decrease in turbine pressure ratio due to an increasing amount of turbine enthalpy at constant compressor power demand and reduced turbine speed.

The differences in turbine efficiency are mainly caused by heat transfer, e.g. to the bearing system at low turbocharger speeds, as a consequence of non-adiabatic turbine operation and mechanical losses at different turbochargers speeds.

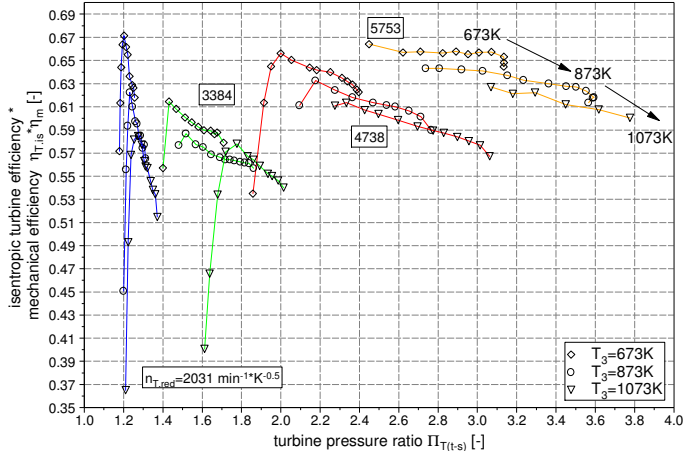


Figure 9: Turbine map – efficiency vs. pressure ratio

The turbine operation implies in detail several loss mechanisms that depend on turbine inlet temperature:

- heat radiation of the turbine casing to the environment [7, 9, 11],
- heat conduction from the turbine to the lubricating oil [8, 11],
- mechanical losses of the turbocharger bearings,
- clearance losses between turbine wheel and casing [10].

The heat radiation is a function of the casing surface area and the fourth potency of the casing surface temperature, whereas the heat conduction from the turbine to the lubricating oil is a linear function of heat flow area and temperature difference of oil and turbine.

The influence of heat transfer from the turbine to the compressor is to be valued less than the heat transfer to the ambient and to the lubrication system. Therefore, the heat conduction from the turbine to the compressor can be omitted [8], [9].

The mechanical losses of the turbocharger bearings are influenced by the turbine inlet temperature, insofar as the turbine map speed parameter is set by the reduced turbine speed

$$n_{T,\text{red}} = n_{TC} \cdot T_3^{-0.5} \quad (11)$$

The turbocharger mechanical efficiency correlates with a quadratic function of the turbocharger speed (when oil is heated up to its specified operating temperatures), but also depends on the thrust load at different turbine pressure ratios.

Generally, the calculation engineer does not have access to the data necessary to define the named dependencies numerically. This suggests use of an empirical expression to qualify turbine maps for alternating turbine inlet temperature.

An analysis of turbine efficiency data on the basis of a large number of turbines mapped at turbine inlet temperatures of

673 K to 1073 K on turbocharger test beds at VOITH Turbo and TU Berlin results in a correlation factor to adjust turbine efficiency values to applied operating conditions e.g. in the exhaust gas path of a Diesel engine. The turbine efficiency correlation factor Z_τ depends on the temperature difference of turbine inlet temperature T_3 to the test bed reference temperature T_{ref} (typically 873 K) and on the turbine impeller diameter d_T (in mm) to take surface area effects into account.

$$Z_\tau = 1 - (T_3 - T_{\text{ref}})(0.0008 \cdot e^{-0.037 \cdot d_T}) \quad (12)$$

The shift of the measured efficiency curves is carried out such as the basic course of the 873 K curve continues without discontinuity. The areas where the compressor operates close to surge or choke cannot be taken into account, because there axial thrust reaches nominal higher values than in the central area of compressor characteristics resulting in a deviation of overall turbine efficiency.

The turbine efficiency of smaller turbines reacts more sensitive to changes of the turbine inlet temperature than larger turbines. This is recognized with the integration of the impeller diameter as a parameter in the definition statement. The correlation factor Z_τ rises with falling turbine inlet temperatures and vice versa.

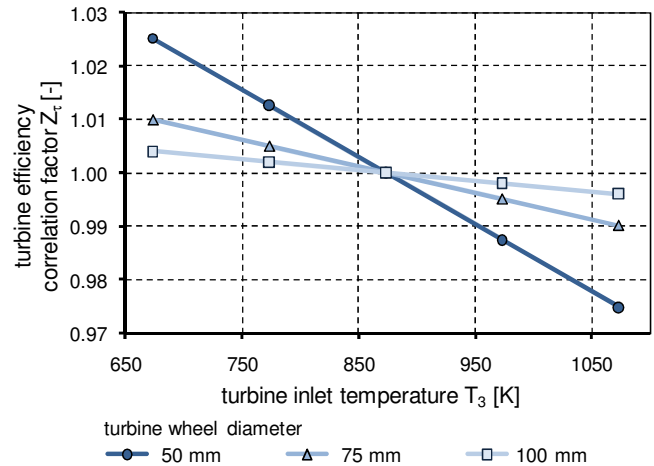


Figure 10: Turbine efficiency correlation factor Z_τ depending on turbine inlet temperature and turbine wheel diameter

According to the existing data basis the equation is valid for turbine inlet diameters d_T from 50 mm to 100 mm. The correlation factor helps to determine turbine efficiency values for typical turbine inlet temperatures that occur in Diesel engines of commercial vehicles (see Figure 2).

ENGINE PROCESS SIMULATION

The following simulation results are prepared with the widely used engine process simulation software GT Power. Therein the pipe flow is modelled one-dimensionally with constant flow variables of flow sections perpendicular to the main flow direction [6]. As described above, turbines are characterised by their maps of turbine flow vs. turbocharger speed and turbine pressure ratio and turbine efficiency vs. turbocharger speed and turbine pressure ratio. Thus, the turbine is comparably modelled as a black box with boundary conditions of the pressure and temperature measurement positions upstream and downstream of the turbine in the hot gas test bed.

The back pressure variation could be modelled by a separation of the standard GT Power turbine templates into a pipe-based volute part and into a map-based turbine wheel part, because performance differences between variants with increased back pressure and with normal back pressure stem from flow modification in the turbine volute. However, this procedure would not be applicable for most engineers because separate turbine wheel maps are usually not available. Thus, a correlation factor based on cycle-averaged values of back pressure is the more applicable alternative.

This factorisation is also applicable for adjustments of effects by variation of the turbine inlet temperature.

Thus, the width of each characteristic can be enlarged by 50 % to 300 % relative to turbine pressure ratio and by 60 % to 500 % relative to blade speed ratio. The rate is larger at higher turbocharger speeds where the compressor map is not as broad as at low turbocharger speeds.

This enlargement of characteristic width provides a broader basis for the extrapolation of turbine characteristics.

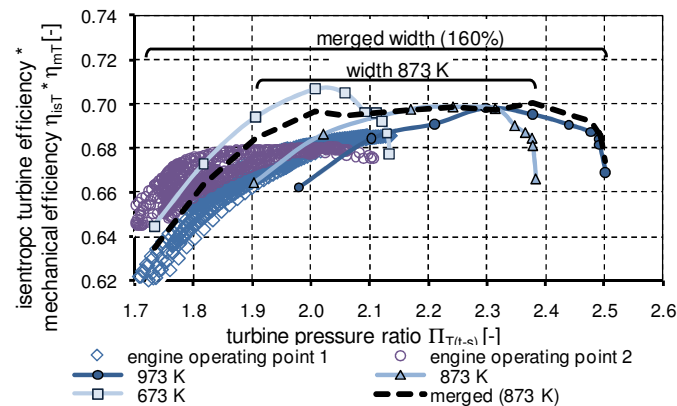


Figure 11: Exemplary correlation of turbine characteristics
 $(n_{T,red} = 3780 \text{ min}^{-1} \text{K}^{-0.5}, d_T = 60 \text{ mm})$

Figure 11 shows an exemplary correlation of a turbine with inlet diameter $d_T = 60 \text{ mm}$ at a reduced turbine speed $n_{T,red} = 3780 \text{ min}^{-1} \text{K}^{-0.5}$. The merged characteristic is based on

measurements with turbine inlet temperatures from 673 K to 973 K. It is formed by reversing equation (12) without respecting the overlapping areas of characteristics mapped with different turbine inlet areas.

In addition, the Figure includes the turbine efficiency distribution of this turbine operating as a high pressure turbine on a two-stage turbocharged 6 cylinder Diesel engine. The engine operates at 50 % load at high speed with 42 % EGR at operating point 1 and at medium speed with 31 % EGR at operating point 2. These instantaneous curves illustrate the use of the characteristic extension. Important areas of the curve, which have not been previously recorded, can now serve as input for the simulation. The instantaneous output data of one combustion cycle deviate slightly from the efficiency input data due to the oscillation of the reduced turbocharger speed.

The results of an exemplary application of turbine back pressure and turbine inlet temperature correlation factors are shown in Figure 12. The engine model consists of a heavy duty 6 cylinder Diesel engine with 0.007 m^3 displacement. The numerical accuracy of the model is proved by consistency between basic simulation model results and test bed results. In the entire engine map the maximum deviation between measured and calculated values is 0.5 % with respect to the air mass flow and 2.4 % with respect to the turbocharger speed.

The implementation of the turbine efficiency correlation factor Z_τ applies to energy-averaged turbine inlet temperatures, because common hot gas test beds provide only data based on constant temperature and flow values.

The consolidated turbine efficiency correlation factor Z is defined by the product of the corresponding factors for turbine inlet temperature Z_τ , defined in equation (12), and turbine back pressure Z_p , defined in Table 4.

$$Z = Z_\tau \cdot Z_p \quad (13)$$

In this particular application, the modelled engine runs with two turbochargers in series where the efficiency correlation with regard to mean turbine inlet temperature multiplied by the efficiency correlation with regard to mean turbine outlet pressure shifts the high pressure turbine efficiency by up to 1.7 % in full load engine operation. The effect on low pressure turbine efficiency is negligible because its operating conditions correspond to the standard turbine test bed conditions.

The overall engine result in brake specific fuel consumption BSFC is lowered by up to 0.16 %.

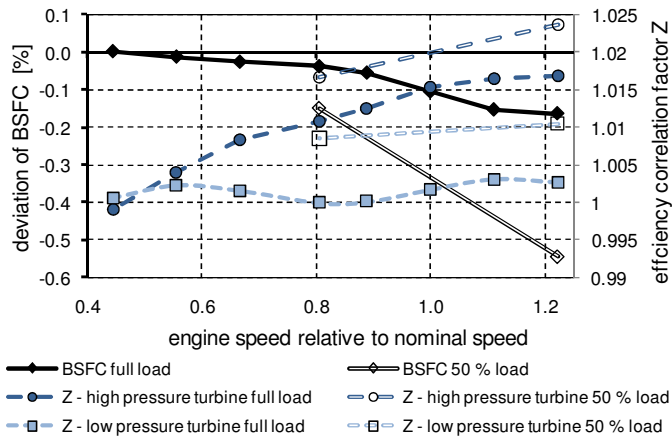


Figure 12: Full load and part load simulation results of a heavy duty Diesel engine

The effect on BSFC is higher at engine part load condition because turbine inlet temperatures are lower than those at engine full load, while high pressure turbine back pressure values stay constant due to the applied high EGR values. Thus, the amount of deviation of BSFC rises to 0.55 %.

The overall impact of the efficiency correlation factor on the general engine performance is lower as expected due to other simplifications e.g. of heat transfer effects or of pulsating flow behavior. The correlation accuracy can be improved substantially by separating the mechanical efficiency from the turbine efficiency so that the effects of inlet temperature and back pressure on mechanical efficiency and isentropic efficiency should be studied isolated. But the general user of turbocharger turbine maps in engine process simulation models has no reliable friction data to map mechanical friction accurately.

CONCLUSION

The turbine efficiency of a radial turbine could be influenced negatively or positively by a variable turbine inlet temperature and by an increased turbine back pressure. This was performed by an experimental programme where different turbines with different capacities were investigated experimentally and numerically.

The investigation shows that an increased back pressure will extend the range of the turbocharger map followed by a simultaneous rise in turbine efficiency. By increasing the back pressure from 1 to 3 bar with constant turbocharger speed, the flow loss in the volute can be reduced, whilst the loss in the turbine wheel is constant. Therefore, the velocity triangles will change only marginally.

Normally a turbine will be investigated on a hot gas test bed with a turbine inlet temperature of 873 K. Decreasing the inlet temperature to lower values leads to a rise in turbine efficiency whereas a rise in the inlet temperature reduces turbine efficiency at constant turbine speed. In this case the effects of an

effects of an increased friction at higher nominal turbocharger speeds, heat transfer to the ambient and to the lubrication oil system dominates and causes a reduction in turbine efficiency. At lower speeds heat transfer will contribute an increase of turbine efficiency.

With the knowledge of the impact of variable turbine inlet temperature and turbine back pressure the turbine maps for a 1D simulation can be improved to generate more realistic results. For an engine with a two-stage charging system, an update in BSFC can be achieved by 0.18 % by raising the turbine efficiency of the high pressure stage by about 1.6 %.

These numbers lead to the statement that the studied effects on overall engine performance cannot be ignored but are often disguised by other model simplifications.

The effects of mechanical efficiency request further research so that the influences of turbine back pressure and turbine inlet temperature on mechanical and isentropic turbine efficiency can be separated consequently. The effects of pulsations in the exhaust system will be investigated in detail by a future research project of the TU Berlin.

REFERENCES

- [1] Baines, A., Wygant, K.D., Dris, A.: *THE ANALYSIS OF HEAT TRANSFER IN AUTOMOTIVE TURBOCHARGERS*, GT2009-59353, ASME Turbo Expo 2009, GT2009, 2009, Orlando
- [2] Bohn, D., Moritz, N. and Wolff, M.: *Conjugate Flow and Heat Transfer Investigation of a Turbo Charger: Part II - Experimental Results*, GT2003-38449, ASME Turbo Expo, 2003, Atlanta
- [3] Otobe, T., Grigoriadis, P., Sens, M., Berndt, R.: *Method of Performance Measurement for Low Turbocharger Speeds*, 9th Conference on Turbochargers and Turbocharging, IMechE, London, 2010
- [4] ANSYS: *ANSYS CFX Help Release 11.0*, 2007
- [5] Baines, N.C.: *Flow Development in Radial Turbine Rotors (96-GT-65)*. International Gas Turbine and Aeroengine Congress and Exhibition Birmingham, UK June 1996
- [6] Gamma Technologies: *GT-SUITE Flow Theory Manual, Version 7.0*, 2009, Westmont
- [7] Shaaban, S.: *Experimental investigation and extended simulation of turbocharger non-adiabatic performance*, Dissertation, Hannover, 2004
- [8] Pucher, H., Mai, H.: *TC-Mapping - Parameterstudie zur Turbolader-Kennfeldvermessung, Abschlussbericht VFI Vorhaben*, 2010
- [9] Berndt, R.: *Einfluss eines diabaten Turboladermodells auf die Gesamtprozess-Simulation abgasturboaufgeladener PKW-Dieselmotoren*, Dissertation, Berlin, 2009
- [10] Watson, N., Janota, M.S.: *Turbocharging the Internal Combustion Engine*, MacMillan Education, London, 1982
- [11] Bohn, D., Heuer, T., Moritz, N., Wolff, M.: *TC-*

*Wärmeströme - Modellierung des Wärmeflusses im und
am System Turbolader, Abschlussbericht FVV-
Vorhaben Nr. 755, 2002*